



## Supporting Information

for *Small*, DOI: 10.1002/sml.201303558

Ultraspecific and Highly Sensitive Nucleic Acid Detection  
by Integrating a DNA Catalytic Network with a Label-Free  
Microcavity

*Yuqiang Wu\**, *David Yu Zhang\**, *Peng Yin*, and *Frank  
Vollmer\**

Copyright WILEY-VCH Verlag GmbH & Co. KGaA, 69469 Weinheim, Germany, 2013.

## Supporting Information

for *Small*, DOI: 10.1002/sml.201303558

### **Ultraspecific and highly sensitive nucleic acid detection by integrating a DNA catalytic network with a label-free microcavity**

*Yuqiang Wu\**, *David Zhang\**, *Peng Yin*, and *Frank Vollmer\**

#### **Immobilization and surface density of DNA probes**

As described in Experimental Section, a layer of biotinylated dextran was physically adsorbed on the cleaned surface of the microspheres. This dextran matrix is proved to be efficient to block any unspecific binding of molecules and effectively increases the surface area to bind more streptavidin molecules than in a surface monolayer. After dextran coating, biotinylated DNA probes were pre-mixed with streptavidin linkers and then immobilized on the microsphere surface. For immobilization we use the ‘hanging drop’ technique: microspheres-on-a-stem are mounted sphere side down on a holder so that a liquid droplet can be added on to the microsphere for incubation during surface coating.<sup>[1]</sup> With this technique, one can easily surface-treat many spheres at the same time using minimal sample solution volumes (~ $\mu\text{l}$ ). The droplets can vaporize, concentrating the solutions and forcing for example streptavidin to occupy the binding sites on the dextran-modified sphere surface.

We can monitor the binding behavior of the DNA probes by injecting the DNA-streptavidin mixture into our droplet cell that contains the dextran coated sphere sensor, here with a diameter of ~ 380  $\mu\text{m}$ . The observed resonance wavelength shift is plotted in Figure S1 and the WGM spectra are shown in the inset. The surface density of the DNA probes at saturation calculated

from the shift in Figure S1 and estimated using Equation 1 is  $\sim 10^{13} \text{ cm}^{-2}$ , at a streptavidin to DNA molar ratio of 1:2, which is consistent with the value calculated from the results of loading the target C or unloading SB (Figure 3). Figure S2 shows the histogram of the saturation probe surface densities for all of the measurements presented in this paper.

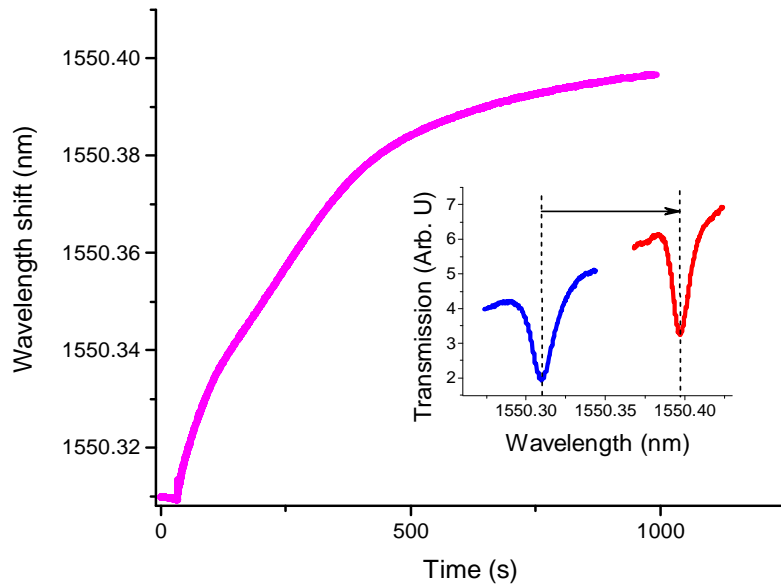


**Figure S1.** Binding of the streptavidin-DNA probe. The streptavidin-DNA pre-mixture was injected into the sample cell at 50 sec. Inset: the spectra of the WGM before (blue) and after (red) the loading of the mixture to a surface density of  $\sim 10^{13} \text{ cm}^{-2}$ .

Assuming that target C hybridizes to all of the streptavidin bound DNA probes immobilized at the surface, we estimate the total amount of target C at  $\sim 83.5 \text{ fmol}$ , multiplying the DNA probe surface density ( $\sim 10^{13} \text{ cm}^{-2}$ ) with the area of the microsphere with a typical diameter of  $400 \mu\text{m}$ . At the detection limit of  $2 \text{ nM}$ , there is a total of  $\sim 800 \text{ fmol}$  target molecules in the droplet sample cell (volume  $\approx 400 \mu\text{l}$ ), which means only  $\sim 10.4\%$  of C is consumed by hybridization and we can approximate the concentration of C to remain constant during the sensing reaction.

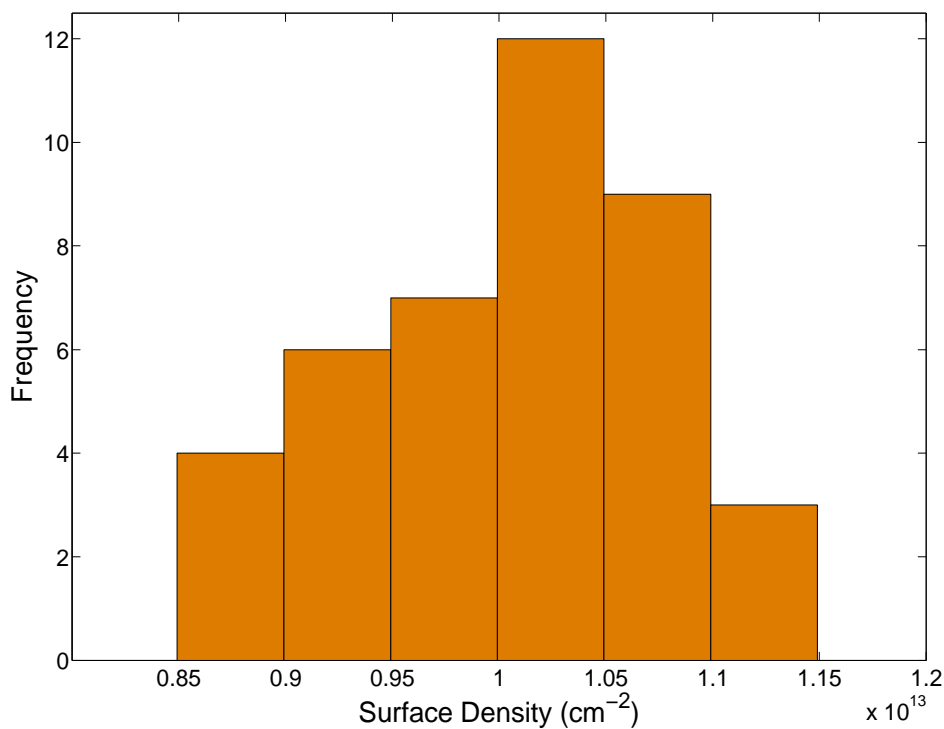


**Figure S2.** Histogram of the DNA probe surface density. Mean value= $(1.00 \pm 0.07) \times 10^{13} \text{ cm}^{-2}$ .

### Polyacrylamide gel electrophoresis (PAGE) for the catalytic network

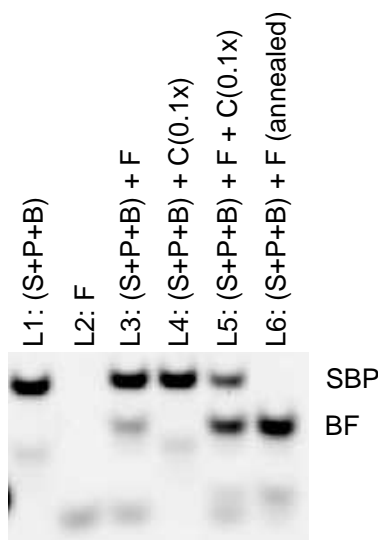


**Figure S3.** Analysis by PAGE of the reaction mechanism shown in Figure 2a. More details on the bulk strand displacement reactions can also be found in refs.<sup>[2]</sup>

### Kinetics of the switch-off catalytic network

To test for recycling of C, experiments have been conducted with a modified sequence Fn which prevents C from being recycled. In the Fn sequence, domain 4 (Figure 2a) was removed from the template sequence F so that once C hybridizes on B, Fn is not able to displace C and the catalysis network is switched off. Results for unloading of the switch-off catalytic network are shown in Figure S4.

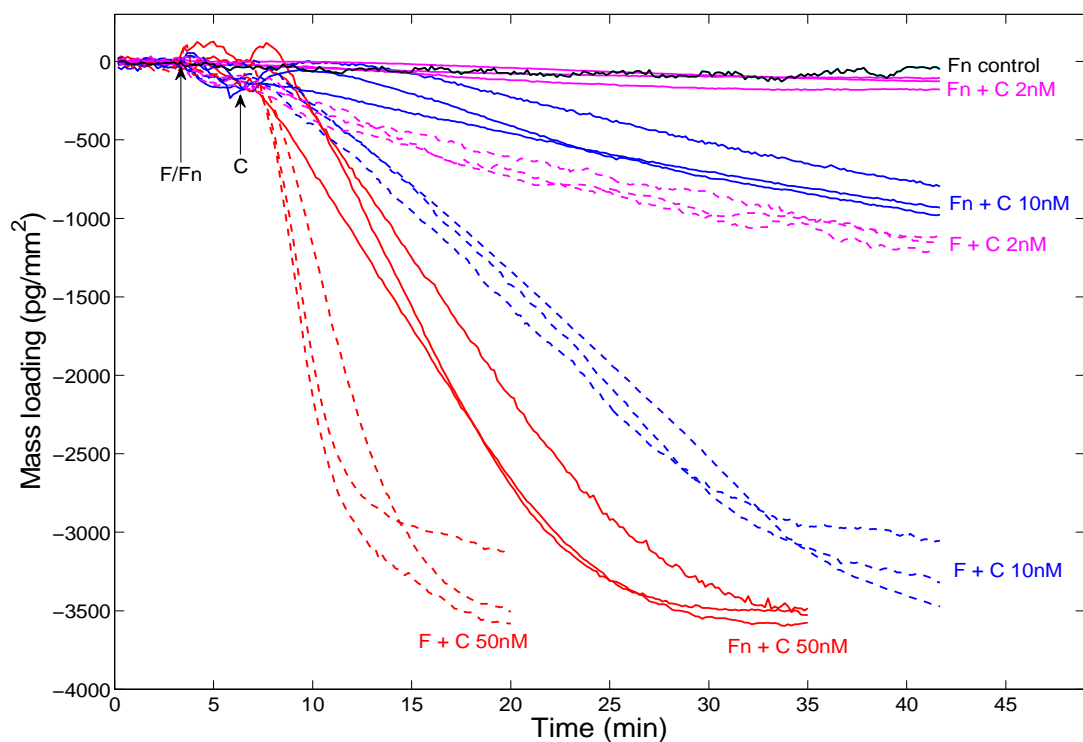


**Figure S4.** Kinetics of the switch-off catalytic network. The dashed lines are re-plotted from Figure 3b. At 200 Sec, 400 nM Fn was injected into the sample cell and at 400 sec, C was injected at concentrations of 50 nM (red), 10 nM (blue) and 2 nM (magenta). Control (black) is done with only Fn injected.

For measurements taken at 2 nM C we confirm that unloading due to catalysis using F (dashed curves) leads to unloading of  $\sim 1100 \text{ pg/mm}^2$  after 45 minutes, whereas unloading without

catalysis using Fn leads to unloading of  $\sim 120 \text{ pg/mm}^2$ , indicating a catalytic turnover of  $\sim 10$  in this case.

**Sensing in complex media: TE Buffer with 10% fetal calf serum**

We challenge the sensor with complex medium, TE buffer (12 mM  $\text{MgCl}_2$ ) with 10% fetal calf serum (FCS). The proteins in FCS bind to the functionalized sensor surface non-specifically (Figure S5) thus potentially blocking some of the pre-attached DNA oligos for subsequent unloading. Unspecific binding of protein can therefore limit the amplitude of our integrated sensor device in nucleic acid detection, however, the sensitivity for detecting target oligonucleotides remains at  $\sim 80 \text{ pM}$  (Figure S6).

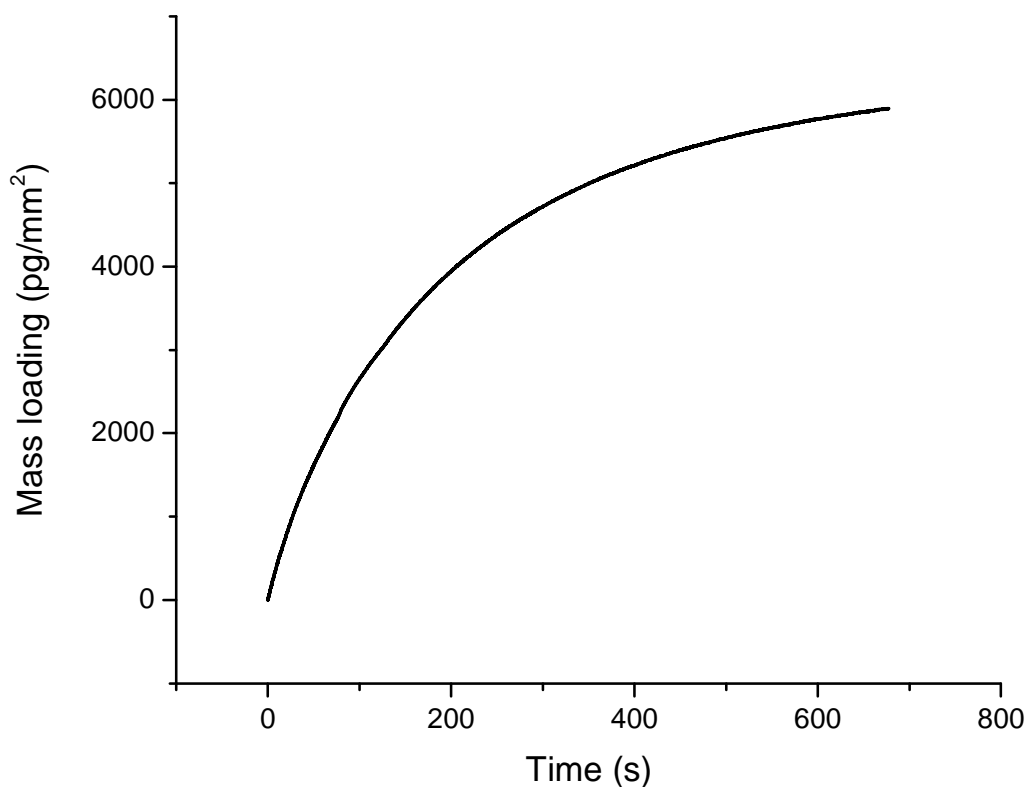


**Figure S5.** Non-specific binding of proteins in FCS.

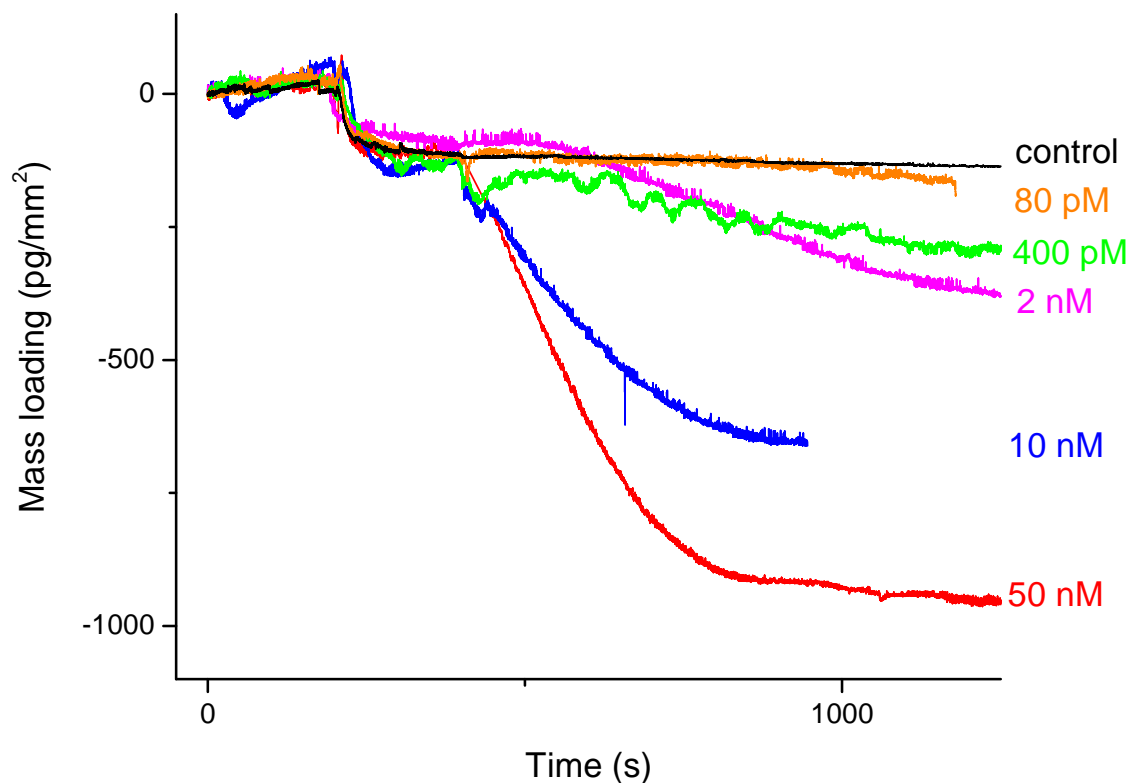


**Figure S6.** The kinetics of the catalytic network in complex media: TE buffer (12.5 mM MgCl<sub>2</sub>) with 10% FCS. At 200 Sec, 400 nM F was injected into the sample cell and at 400 sec, C was injected at concentrations of 50 nM (red), 10 nM (blue), 2 nM (magenta) 400 pM (green) and 80 pM (orange). Control (black) is done with only F injected.

### Characterization of the S2B2F2C2 catalytic network

To test the versatility of the integrated sensor, a second catalytic network has been designed. The second network shares the same probe DNA strand, P, but the other strands are different, labeled as S2, B2, F2, and C2 (target). The kinetics of the second network is shown in Figure S7 and is slower than the first network. As discussed in the main paper, this is due to the significant secondary structure in F2, as determined by DNA folding software. This is generally known to inhibit hybridization and strand displacement reactions. Nonetheless, even with this non-ideal sequence setup, C2 is still reliably detected by the WGM strand-displacement sensor.

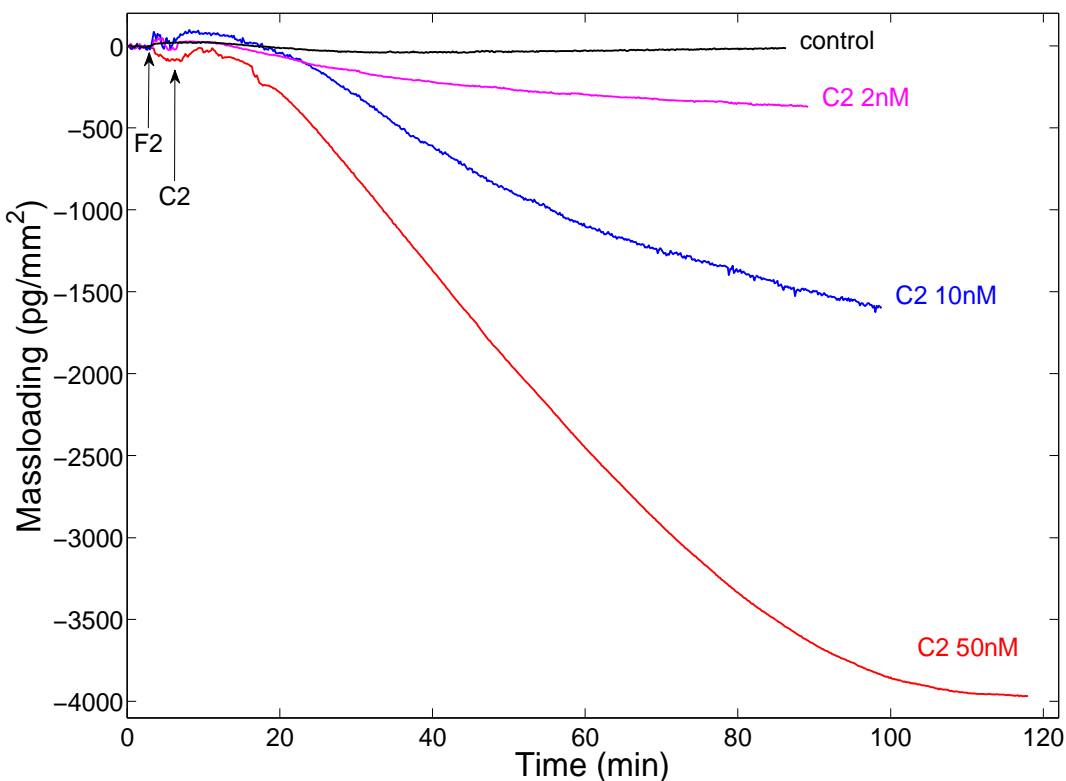


**Figure S7.** The kinetics of the second network. At 200 Sec, 400 nM F2 was injected into the sample cell and at 400 sec, C2 was injected at concentrations of 50 nM (red), 10 nM (blue) and 2 nM (magenta). Control (black) is done with only F2 injected.

### Reusability

After one measurement, both sequences S and B are released from the sphere surface leaving the biotinylated strand P available for hybridization. Therefore, the same WGM microsphere can be regenerated simply by hybridizing the sequences S and B back on the microsphere surface. In Figure S8, we show that one integrated WGM sensor can be used in 3 successive cycles of detection. After each loading/unloading experiment, the microsphere-taper system was taken out from the droplet sample cell and then immersed back into the cell after replacing the buffer

solution in a new droplet. This leads to some arbitrary offset of the WGMs during buffer exchange. After the microsphere sensor has been put in the next droplet cell and equilibrium state has been reached, we recorded the relative shift of the WGMs. Mass loading is determined by Equation 1 and the curve is offset so that the next loading/unloading cycle starts where the last one has ended.

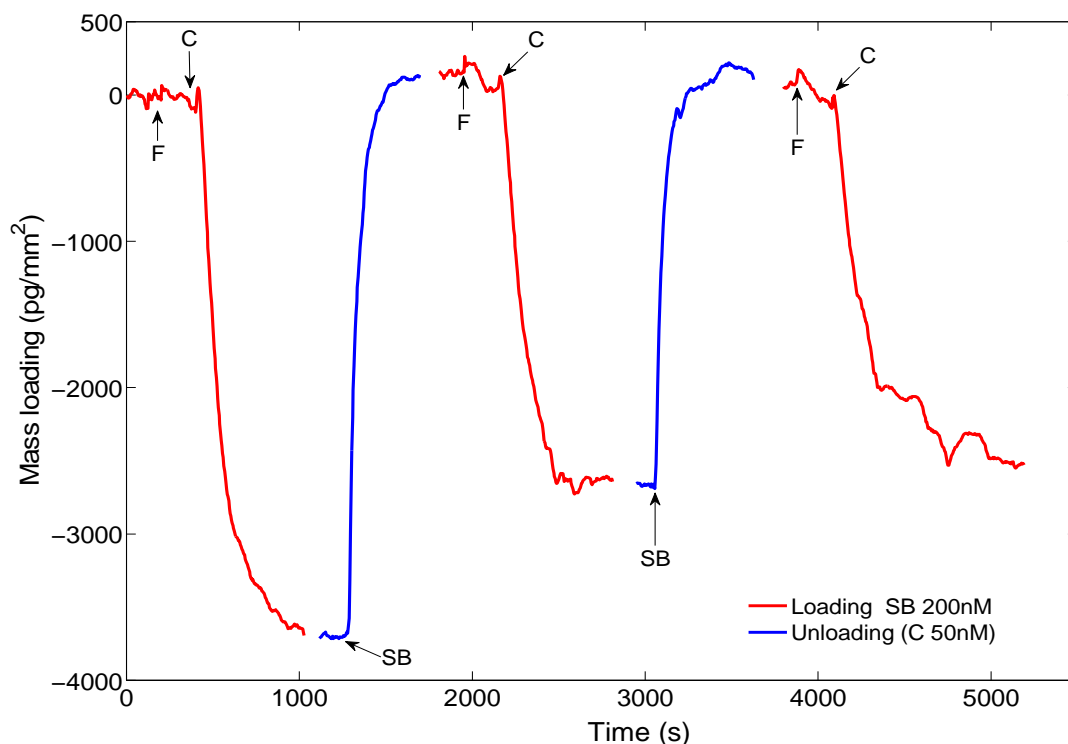


**Figure S8.** Regeneration of the WGM sensor using the S, B, F, C network. The unloading experiments were performed with 400 nM of F and 50 nM of C while the sequences S and B were loaded back at a concentration of 200 nM each.

### Detection limit of WGM sensor by direct hybridization

To confirm that the detection limit of the WGM microsphere sensor under the direct hybridization is  $\sim 2$  nM, we have designed and tested another probe-target pair, T\* and T (see Figure 9). The results are consistent with Figure 3a, which shows very similar kinetics for C\* and C.

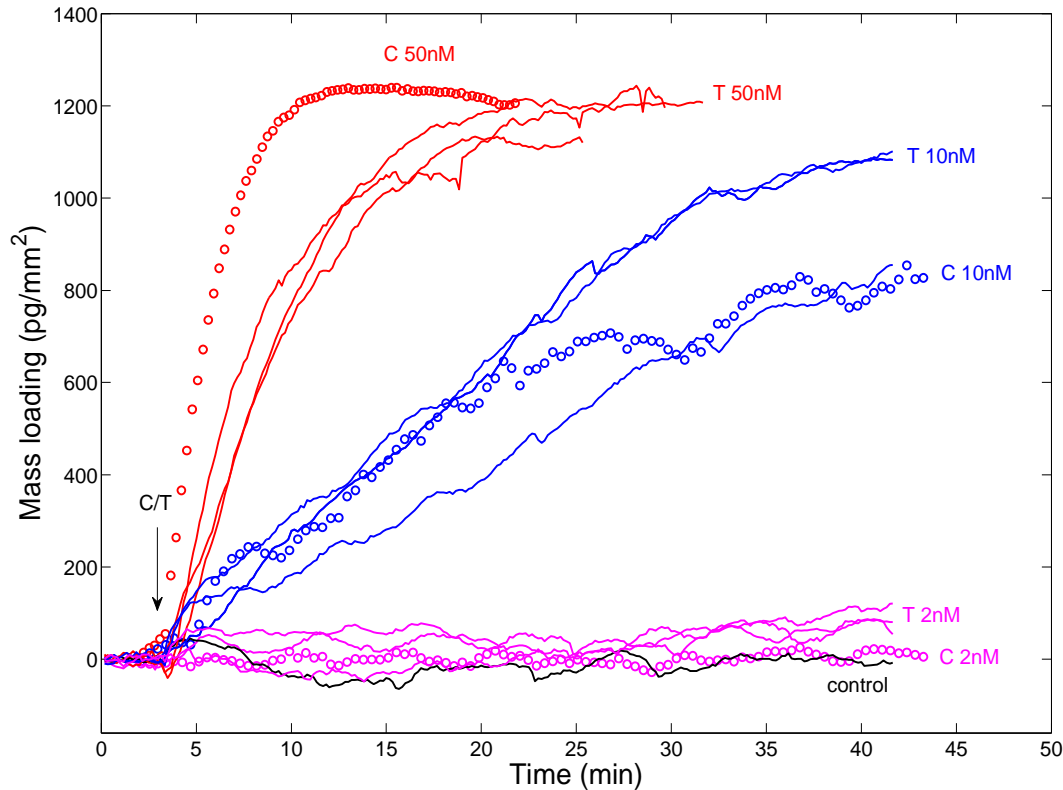


**Figure S9.** Kinetics of hybridization of T onto the pre-attached probe T\*. T was injected into the sample cell at 200 sec, with concentrations of 50 nM (red), 10 nM (blue) and 2 nM (magenta). Control experiments (black) were done by immersing the sensors in the sample cell without injecting anything.

### Q-factor and coupling efficiency of the WGM microcavities

The loss of the WGM microcavity is the most important figure of merit, which is commonly expressed in terms of the quality factor (**Q**), given by  $Q = \lambda / \Delta\lambda_{\text{line}}$ , where  $\Delta\lambda_{\text{line}}$  is the linewidth determined at FWHM. The Q-factors of the WGMs monitored from spectra shown in Figure S2 is shown in Figure S10. The Q-factors are on the order of  $3 \times 10^5$ . We note that the Q factor has no bearing on the magnitude of the mass loading signal but instead determines how accurate a resonance wavelength shift signal can be resolved from recordings of WGM spectra.<sup>[3]</sup>

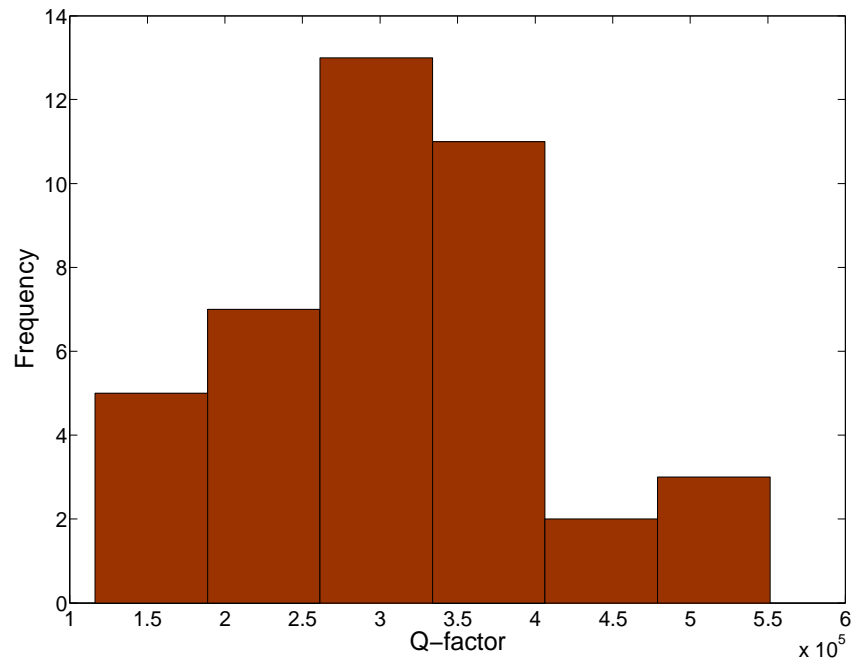


**Figure S10.** Q-factor histogram of the WGMs that were monitored in Figure S2. Q-factor mean value =  $3.1 \times 10^5$ .

The coupling efficiency,  $e$ , which represents how much power is coupled into the microsphere, is calculated by  $e = 1 - T_0/T_s$ , where  $T_0$  and  $T_s$  are the transmitted power with and without the microsphere, respectively. The coupling efficiencies of the WGMs that were monitored in Supplementary Figure 2 and 8 are shown below. We note that the coupling efficiency has no bearing on the magnitude of the mass loading signal.<sup>[3]</sup>

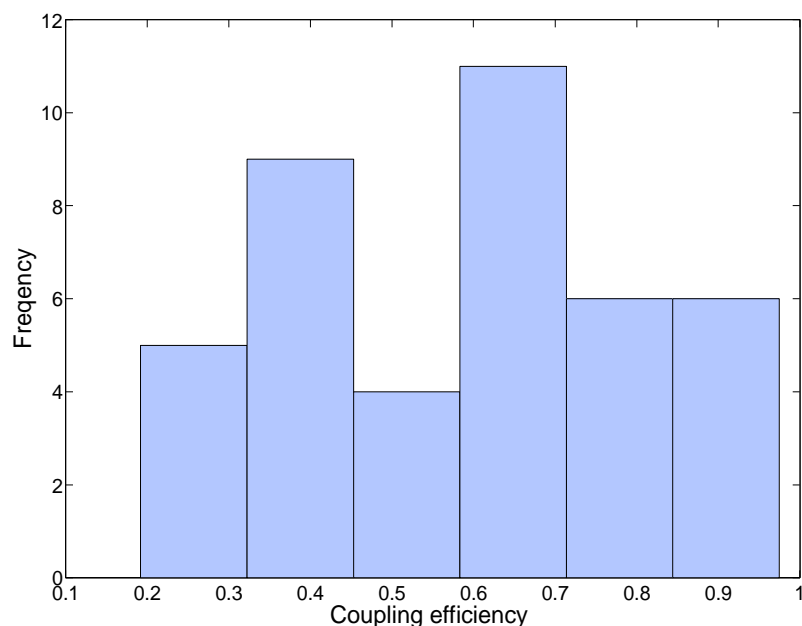


**Figure S11.** Coupling efficiency histogram of the WGMS that were monitored in Figure S2.

### Sequences of the oligonucleotides

**Table S1.** Sequences of the oligonucleotides involved in the catalytic network and the direct hybridizations.

Domain	Sequences	Length (nt)
<b>Fn</b>	5'-CTGTA CACTAAAGTTCCTACC-3'	21
<b>C2</b>	5'-TGTAACAGCAACTCCATGTGGA-3'	22
<b>S2</b>	5'-GCAACTCCATGTGGACTGTA-3'	20
<b>B2</b>	5'-GCGATG GGTAAGAACTTTAGTG TACAG TCCACATGGAGTTGC TGTTACA-3'	49
<b>F2</b>	5'-GCAACTCCATGTGGA CTGTA CACTAAAGTTCCTACC-3'	36
<b>T</b>	5'-CCCTATAGTGAGTCGTATTAAT-3'	22
<b>T*</b>	5'-biotin-ATTAATACGACTCACTATAGGG-3'	22

### Data processing

To calculate the initial slope of the DNA binding/unloading, we fit an exponential curve<sup>[4]</sup> as described by:

$$M(t) = A[1 - e^{-B(t-t_0)}](S1)$$

The initial slope of the binding/unloading isotherm is given by the derivative of Equation S1

evaluated at  $t = t_0$  :

$$\frac{dM}{dt} = AB$$

An average of the initial slopes was taken over a number of sensors,  $n$ , for each concentration and the standard deviations were used as the error bars in Figure 2c. For 50 nM concentration, Equation S1 was used to approximate the initial slopes while for lower concentrations a linear fit was used since the sensor response was sufficiently slow. As a general rule, the first 15 min of collected data after the injection of the target was used to obtain a fit. For the SNP variants experiments, we use the 15 min of data when the unloading started for fit. The fitting parameters used for all measurements are included in Tables S2-S9. All data was fitted using OriginPro8 (OriginLab Corporation).

### Parameters from data fitting

**Table S2.** Parameters for the **exponential** fit to the data of 50 nM hybridization shown in Figure 3a.

Concentration (nM)	A (pg/mm <sup>2</sup> )	B (s <sup>-1</sup> )	t <sub>0</sub> (s)	AB(pg/mm <sup>2</sup> s)	R <sup>2</sup>
50	1259.9194	0.00653	-1.7908	8.227	0.99727
	1210.9568	0.00446	0.33414	5.401	0.99984
	1248.4708	0.00468	12.5500	5.843	0.99938

**Table S3.** Parameters for the **exponential** fit to the data of 50 nM unloading shown in Figure 3b.

Concentration (nM)	A (pg/mm <sup>2</sup> )	B (s <sup>-1</sup> )	t <sub>0</sub> (s)	AB (pg/mm <sup>2</sup> s)	R <sup>2</sup>
50	-3093.3140	0.00425	23.1719	13.147	0.99013
	-3718.3051	0.00479	30.5821	17.811	0.98548
	-4272.9731	0.00245	38.7121	10.469	0.98025
	-328773	0.0051	29.5379	16.574	0.97589

**Table S4.** Parameters for linear fit to the data of hybridization shown in Figure 3a.

Concentration (nM)	Slope (pg/mm <sup>2</sup> s)	Intercept (pg/mm <sup>2</sup> )	R <sup>2</sup>
10	0.55476	41.51352	0.95491
	0.33585	35.14786	0.92105
	0.39598	100.7102	0.93805
	0.62894	58.98142	0.96953
2	0.01257	-7.02465	0.3311

---

	0.1152	-15.63048	0.88576
	0.0999	-3.30821	0.93817
<b>Control</b>	-0.04707	19.4324	0.57823
	-0.0084	11.3684	0.35963
	-0.01892	14.4823	0.49493

**Table S5.** Parameters for linear fit to the data of unloading shown in Figure 3b.

---

Concentration (nM)	Slope (pg/mm <sup>2</sup> s)	Intercept (pg/mm <sup>2</sup> )	R <sup>2</sup>
<b>10</b>	-1.8959	-29.4227	0.99752
	-1.6624	12.6604	0.99552
	-2.9450	102.8044	0.99675
	-1.8679	96.7972	0.99733
<b>2</b>	-0.6796	-208.211	0.98454
	-0.5893	-149.131	0.98759
	-0.7437	-134.426	0.97113

---

<b>0.4</b>	-0.4602	-96.221	0.97824
	-0.4880	-128.643	0.97212
	-0.2779	-84.330	0.93987
<b>0.08</b>	-0.0773	-49.657	0.74311
	-0.2408	-36.678	0.97494
	-0.2110	-88.219	0.91568
	-0.1635	-49.408	0.88618
<b>Control</b>	-0.0596	-8.9788	0.35735
	-0.0086	-106.464	0.36080
	-0.0262	21.794	0.49905

**Table S6.** Parameters for linear fit to the data of 50 nM SNP variants unloading shown in Figure 4b.

SNP variants	Slope (pg/mm <sup>2</sup> s)	Intercept (pg/mm <sup>2</sup> )	R <sup>2</sup>
<b>Cm5aG</b>	-0.3141	340.055	0.83029
	-0.3279	121.122	0.99221

	-0.4711	247.963	0.98819
<b>Cm11cT</b>	-0.1401	380.905	0.56489
	-0.1225	271.624	0.93732
	-0.1136	154.016	0.94761
<b>Cm14gC</b>	-0.0684	7.8741	0.59934
	-0.0770	279.3374	0.95884
	-0.0518	117.628	0.92245

**Table S7.** Summary of initial slopes used in Figure 3a.

Concentration (nM)	N (number of measurements)	Mean initial slope (pg/mm <sup>2</sup> s)	Standard deviation of mean (pg/mm <sup>2</sup> s)
50	3	6.490	1.241
10	4	0.479	0.118
2	3	0.0759	0.0452
Control	3	-0.0248	0.0163

**Table S8.** Summary of initial slopes used in Figure 3b.

Concentration	N (number of	Mean initial slope	Standard deviation of mean
---------------	--------------	--------------------	----------------------------

(nM)	measurements	(pg/mm <sup>2</sup> s)	(pg/mm <sup>2</sup> s)
50	4	-14.50	2.89
10	4	-2.093	0.500
2	3	-0.671	0.064
0.4	3	-0.409	0.093
0.08	4	-0.173	0.062
Control	3	-0.0315	0.021

**Table S9.** Summary of initial slopes used in Figure 4b.

SNP variant	N (number of measurements)	Mean initial slope (pg/mm <sup>2</sup> s)	Standard deviation of mean (pg/mm <sup>2</sup> s)
Cm5aG	3	-0.371	0.0709
Cm11cT	3	-0.126	0.0108
Cm14gC	3	-0.0657	0.0105

- [1] F. Vollmer, S. Arnold, D. Braun, I. Teraoka, A. Libchaber, *Biophys. J.* **2003**, *85*, 1974.
- [2] D. Y. Zhang, A. J. Turberfield, B. Yurke, E. Winfree, *Science*. **2007**, *318*, 1121.
- [3] F. Vollmer, S. Arnold, *Nat. Methods* **2008**, *5*, 591.
- [4] A. J. Qavi, R. C. Bailey, *Angew. Chemie-International Ed.* **2010**, *49*, 4608.